Materials Advances

ROYAL SOCIETY OF CHEMISTRY

PAPER

View Article Online
View Journal | View Issue

Cite this: *Mater. Adv.*, 2023, 4, 2214

N,N′-Substituted quinacridones for organic electronic device applications†

Donia Saadi,‡[ab] Felix Mayr,‡[ac] Cigdem Yumusak,[a] Dominik Wielend,[a] Munise Cobet,[a] Bilge Kahraman,[a] Cristian Vlad Irimia,[a] Yasin Kanbur,[ad] Mateusz Bednorz,[a] Kamil Kotwica,[aef] Amel Ben Fredj,[b] Samir Romdhane,[b] Markus C. Scharber,[a] Niyazi Serdar Sariciftci[a] and Mihai Irimia-Vladu*[a]

Received 2nd November 2022,
Accepted 3rd April 2023

DOI: 10.1039/d2ma01010k

rsc.li/materials-advances

N,N′-Substituted quinacridones are a novel class of commercially available quinacridones for organic electronics which are reported here. In this study, we performed in-depth investigations of the material properties of these molecules *i.e.* their optical and charge transport properties, infrared-active vibrations (FTIR), electrochemical reduction and oxidation properties, thin film forming and processability, and finally performance in organic field effect transistor devices. We show that substitution plays a critical role in the charge transport properties, with methyl substituted amine being the most favorable, followed by di-phenyl and finally di-butyl.

Introduction

The electronics industry progressed from heavy and bulky devices to smart, mobile appliances that considerably changed our life.[1,2] Traditional electronic devices today rely on inorganic insulators, semiconductors and conductors, like silicon dioxide, silicon and gold as conventional materials.[3] They are however rigid and stiff in their mechanical properties, precluding them from an intimate integration in our body and on textiles.[4–6] Carbon based organic electronics in contrast to traditional electronics enable the fabrication of extremely flexible, highly conformable and even imperceptible electronic devices.[7] Such properties stimulate ground-breaking applications that may lead to new mainstream solutions in information and communication technology such as ambient intelligence for daily-life assistance,[8,9] soft robotics and actuators,[10] conformable and self-sustaining bioelectronic components for sports and recreation,[11–13] as well as imperceptible electronic platforms for surgical and diagnostic implants.[14–22] Materials that are easy to synthesize in high yield at low cost[23] and that have widespread application as textile or cosmetic colors are very appealing for the development of sustainable organic electronic devices and integrated sensors.[9,24,25] In our quest of investigating dyes and pigments of industrial relevance for organic semiconductors, we selected three molecules in the family of quinacridone pigments due to their straight forward synthesis and large-scale availability.[23] Quinacridone and its derivatives are interesting semiconductor materials as they feature intramolecular hydrogen bonds that planarize them in molecular packing and render long range order arrangement in the solid state.[26,27] Even though they have limited π–π-conjugation within the individual molecule, they are robustly packed in the condensed phase, presumably due to the inter-molecular H-bonds. In solid films, compared to individual molecules in solution, their semiconductor band gap decreases dramatically and an extensive, highly stable inter-connected π-conjugated network with excellent charge transport properties is formed.[20,28–31] In addition to their already reported electronic properties, polycyclic organic molecules like quinacridones were also identified as efficient electrocatalysts for oxygen to hydrogen peroxide reduction.[32]

We selected in this study three quinacridone molecules for which the intramolecular hydrogen bonding is disrupted due to the substitution at the *N,N′* positions of the respective molecules. The selected groups, methyl, butyl and phenyl, have an impact not only on the spectroscopic and electrochemical properties, but also on the arrangement of molecules in the layer. As a matter of fact, among the three selected substitutions to the

[a] *Linz Institute for Organic Solar Cells (LIOS), Institute of Physical Chemistry, Johannes Kepler University Linz, Altenberger Str. 69, 4040, Linz, Austria. E-mail: mihai.irimia-vladu@jku.at*
[b] *Laboratoire Matériaux Avancés et Phénomènes Quantiques, Faculté des Sciences de Tunis, Université de Tunis El Manar, Campus Universitaire, Tunis 2092, Tunisia*
[c] *Institute of Applied Physics, Johannes Kepler University Linz, Altenberger Str. 69, 4040 Linz, Austria*
[d] *Department of Chemistry, Karabük University, Baliklarkayasi Mevkii, 78050 Karabük, Turkey*
[e] *Institute of Physical Chemistry, Polish Academy of Sciences, Kasprzaka 44/52, 01-224 Warsaw, Poland*
[f] *Faculty of Chemistry, Warsaw University of Technology, Noakowskiego 3, Warszawa, 00-664, Poland*

† Electronic supplementary information (ESI) available. See DOI: https://doi.org/10.1039/d2ma01010k

‡ These authors contributed equally.

parent quinacridone molecule, *N*,*N*′-dimethyl quinacridone was recently reported as a solid-state emissive dye with a mechanochromic luminescence[33] and as a binder to a polyaromatic cage for the development of molecular sensors;[34] whereas dibutyl quinacridone was recently implemented as a photothermal evaporator for solar steam and thermoelectric power generation,[35] and also used as a precursor for the synthesis of a novel quinacridone dye for organic dye-sensitized solar cell applications.[36] Nevertheless, it is worth pointing out that the attempt to fabricate field effect transistors with *N*,*N*′-dibutyl quinacridone semiconductors on a classic octadecyltrichlorosilane capped silicone dioxide dielectric proved unsuccessful.[37] It was also recently reported that the introduction of an alkyl or aryl substituent caused a bathochromic shift in the absorption and emission spectra.[38–40] By analyzing the substituent effect on acenes, including pentacene, it was confirmed that the location and type of group change not only the electrochemical or spectroscopic properties,[41] but also the arrangement of the molecules of the oriented semiconductor layer, which translates into the mobility of the charge in these layers.[42] On fundamental grounds, this comparative study aims at understanding whether there is an electronic effect in OFETs for these H-bonded dyes with the disruption of intramolecular conjugation *via* substitution at the amino positions. The stability and availability of these organic semiconductor materials are the primary motivation for choosing to investigate them in OFET devices.

Experimental

All the investigated small molecules in this work were subjected to a scrupulous purification process, using a method reported previously by our group.[43] With this respect, each material has been purified by two successive temperature gradient sublimations using a quartz vacuum tube at a *p* pressure of approximately 1×10^{-6} mbar. Two borosilicate glass tubes inserted into the quartz tube served both as a confinement of the source material and as a vehicle for retrieving the sublimed material. Each of the three materials sublimed in a 24 h period at a particular temperature: 240 °C for DBQA, 280 °C for DPQA and 290 °C for DMQA. More insight into the purification process of organic materials is given in our recent publication dealing specifically with the importance of purity for the improvement of organic semiconductor performance.[43]

Cyclic voltammetry (CV) was performed using a Vertex One Ivium potentiostat/galvanostat inside a nitrogen (N_2) filled glove box. As an electrochemical cell, a one-cell compartment with 150 nm evaporated thin films of the respective material on ITO/glass (Xin Yan Technology LTD) was used as a working electrode, platinum as a counter electrode and an Ag/AgCl electrode as quasi-reference electrode. A 0.1 tetrabutylammonium hexafluorophosphate ($TBAPF_6$, >99.0%, Sigma Aldrich) in acetonitrile (MeCN, >99.9%, Roth) was used as an electrolyte solution. The CV scans were performed separately for reduction and oxidation at a scan rate of 20 mV s^{-1} and the onset potentials were determined *via* tangents. In order to convert the applied potential *versus* the standard hydrogen electrode (SHE), after each measurement, a calibration with ferrocene (98%, Sigma Aldrich) was performed. Re-calculation of the potential was done using the literature value of the ferrocene potential $E_{1/2}$ = +0.640 V *vs.* SHE.[44]

Fourier-transform infrared (FTIR) spectra were recorded using a Bruker Vertex 80 FTIR spectrometer equipped with a Bruker Platinum attenuated total reflectance (ATR) unit. The spectra were recorded with a resolution of 1 cm^{-1} and averaging 200 scans. The measurements were performed on the powders of the *N*,*N*′-substituted quinacridone materials after purification by vacuum sublimation.

UV-Vis absorbance spectra were measured using a PerkinElmer Lambda 1050 spectrophotometer. Photoluminescence (PL) spectra were measured using a Photon Technology International Quanta Master 40 spectrofluorometer with a dual monochromator arrangement in both the excitation and the emission channel, respectively. Absorbance and PL measurements were performed on dilute solutions of the *N*,*N*′-substituted quinacridones in dimethyl sulfoxide (DMSO, concentrations of *ca.* 10^{-5} M) and on thin films of the respective materials deposited on quartz glass *via* thermal evaporation. Time-resolved photoluminescence measurements were performed on the same solutions and thin films on quartz using time-correlated single photon counting (TCSPC). The TCSPC setup consisted of a Becker & Hickl SPC 150 TCSPC module, a PMC-100-1 photomultiplier, a DeltaNu DNS-300 monochromator (slit widths: 1 mm), and an NKT Photonics SuperK FIANIUM FIU-15 as excitation light source equipped with a pulse picker and a Photon Etc LLTF Contrast VIS wavelength selection unit.

For structural characterization of the films, an MRD (Materials Research Diffractometer, PANalytical X-Pert) was used to record 2θ–ω-scans with a horizontal goniometer (320 mm radius) in a four-circle geometry working with the K_α-line of a ceramic X-ray tube anode (λ = 1.540 Å). The MRD is equipped with the different incident and diffracted optics which can be interchanged depending on the application required (here: a Ge(440) four-crystal monochromator). A PIXcel detector, which is a fast X-ray detector based on "Medipix^2" technology with a 256 × 256 pixels array, was used. The measurements were done with a resolution of 0.05° and an accumulation time of 1.76 s by using a divergence slit fixed to 0.38 mm.

Transistors were fabricated in a staggered bottom gate-top contact geometry on glass substrates, with a 100 nm thick aluminum gate electrode whose surface was superficially anodized electrochemically to AlO_x for ~18 nm thick aluminum oxide layer, through a reported method.[45,46] The aluminum oxide layer was subsequently capped by a thin layer of vacuum-deposited tetratetracontane (TTC) of 20 nm for dimethyl- and dibutylquinacridone and ~12 nm beeswax (doctor bladed from 2 mg ml^{-1} solution in chloroform) for diphenylquinacridone.[47,48] While it is known that various film deposition conditions of quinacridone molecules generate different polymorphs that are drastically different from one another in molecular packing and transport properties, we did not pursue the avenue of identification of individual polymorphs resulting from the vacuum deposition conditions.[28,49,50] The gold source and drain electrodes

were deposited *via* physical vapor deposition, with channel dimensions of width, W = 2 mm and length, L = 25 μm. We fabricated 3 batches of 6 slides per batch, 4 OFETs per slide for each of the three *N*,*N*′-substituted quinacridone molecules.

Results and discussion

The schematic of the three quinacridone derivatives, substituted in the *N*,*N*′ positions, that feature limited intramolecular hydrogen bonding compared to linear trans quinacridones is presented in Fig. 1. They are dimethyl-, dibutyl- and diphenylquinacridone(s), all of them are commercially available. We purchased *N*,*N*′-dimethyl quinacridone (DMQA) and *N*,*N*′-dibutylquinacridone (DBQA) from TCI and *N*,*N*′-diphenylquinacridone (DPQA) from Synthon Chemicals GMBH & Co KG.

According to the electrochemical measurements shown in Fig. 2, all three materials investigated display distinct oxidation and reduction characteristics. Despite differences in the measured current, resulting because of the different electrode areas in contact with the electrolyte solution, all three compounds have a comparable reduction potential (LUMO) of around −1.2 V *vs.* SHE. Comparison of the oxidation features revealed nonetheless a significant difference among them, in the sense that DMQA and DPQA possess two irreversible oxidation peaks, while DBQA only possesses one oxidation peak. Regarding the oxidation potentials, the substituents on the nitrogen atoms have a significant influence as the oxidation reaction is expected to occur there. Thereby variations of the HOMO levels by 120 mV were observed, which are as a matter of fact the main contributors to the difference in band gaps determined from cyclic voltammetry for the three compounds. With this respect, we calculated band gaps of 2.54 eV, 2.57 eV and 2.64 eV for DMQA, DBQA and DPQA, respectively. Comparison of our electrochemical potentials in the case of the *N*,*N*′-dibutylquinacridone reveals a very good correlation to the results reported by Zhang *et al.*,[51] even though they were recorded in homogeneous solutions and they calculated the reduction potential from the oxidation potential and the optical band gap. Literature reports on HOMO–LUMO levels of DMQA from Socol *et al.*[52] and Leem *et al.*[53] show some moderate deviation from our results, although it has to be mentioned that in contrast to this present work, they used photoelectron spectroscopy for the determination.

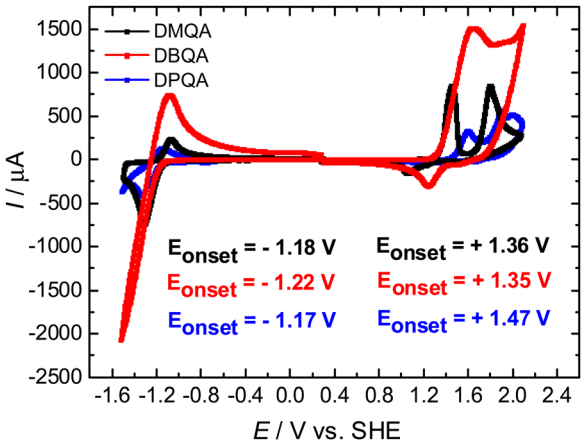

Fig. 2 Cyclic voltammograms of *N*,*N*′-substituted quinacridones. The onsets of reduction and oxidation reactions are displayed as insets in the graph.

The ATR-FTIR spectra measured for the powders of the three *N*,*N*′-substituted quinacridone derivatives are shown in Fig. 3. The wavenumbers and assignments of selected characteristic IR absorption bands of the compounds as determined from the FTIR spectra are summarized in Table 1. The spectra of the three differently substituted quinacridones largely show high conformity of the wavenumbers and relative intensities of the main infrared absorption bands such as the carbonyl stretching vibrations and the aromatic ring stretching vibrations. The spectra measured for our DMQA and DBQA samples conform well to the spectra reported in the literature.[49,54] When comparing the FTIR spectra of the three compounds, some characteristic differences can be observed which can be related to the different substituents at the nitrogen atoms. While all three spectra show C–H stretching vibration bands of the C–H bonds in the aromatic rings above 3000 cm^{-1}, the occurrence of saturated hydrocarbon C–H stretching bands at wavenumbers below 3000 cm^{-1} can only be observed for dimethyl- and dibutyl-substituted quinacridone. These bands can be attributed to the alkyl substituents. The difference in the alkyl chain length between the methyl and butyl group is shown by the larger relative intensities of these bands for

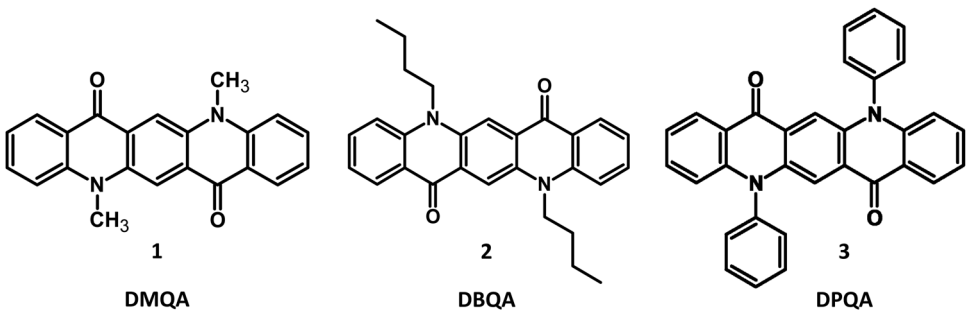

Fig. 1 Chemical structures of the *N*,*N*′-substituted quinacridone molecules: (**1**) *N*,*N*′-dimethylquinacridone (5,12-dimethylquinolino[2,3-*b*]acridine-7,14-dione); (**2**) *N*,*N*′-dibutylquinacridone (5,12-dibutylquinolino[2,3-*b*]acridine-7,14-dione); (**3**) *N*,*N*′-diphenylquinacridone (5,12-diphenylquinolino[2,3-*b*]acridine-7,14-dione).

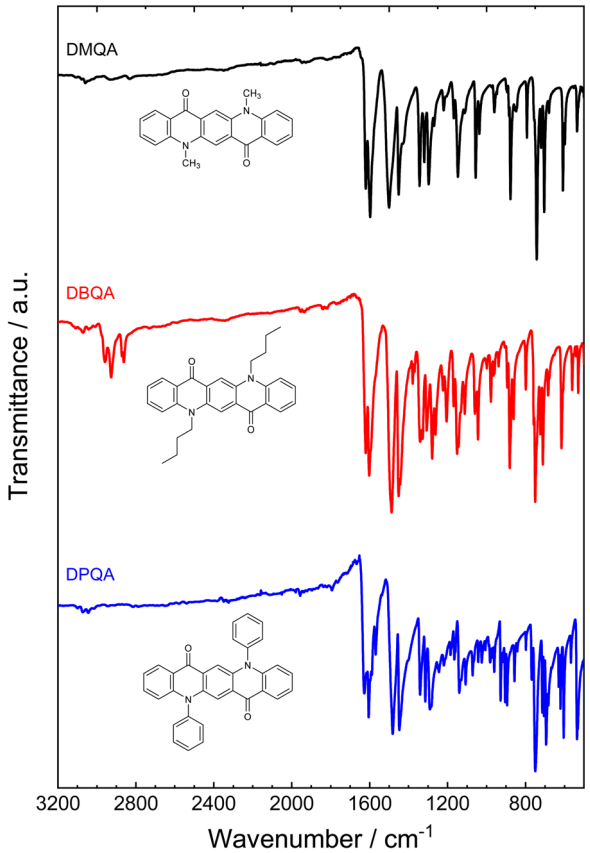

Fig. 3 ATR-FTIR spectra measured for the powders of the three *N,N′*-substituted quinacridone derivatives after purification by vacuum sublimation.

DBQA. Additional bands of strong to medium intensity which can be related to the C–H bending vibrations of the alkyl substituents can also be observed at wavenumbers of 1443 cm^{-1} and 1428 cm^{-1} for DBQA and DMQA, respectively. For DPQA on the other hand, an additional aromatic C═C stretching absorption band at 1569 cm^{-1} as well as a strong phenyl ring deformation band at 536 cm^{-1} are present. The FTIR spectra confirm the presence of the different substituents at the N atoms in the quinacridone derivatives and indicate that no degradation or loss of the substituent groups occurred upon purification by vacuum sublimation.

Fig. 4 shows the UV-Vis absorbance and photoluminescence spectra of the three *N,N′*-substituted quinacridone derivatives measured for dilute solutions in DMSO and for thin films of the materials on glass. The absorbance spectra of all three investigated compounds in the DMSO solution show a progression of three absorption bands in the visible light range with decreasing intensity towards lower wavelengths. The bands can be attributed to the 0-0, 0-1 and 0-2 transition to the corresponding vibrationally excited sublevel of the S_1 excited state, respectively.[58,59] All three compounds show nearly identical intensities of the vibronic absorption bands relative to the 0-0 transition. For *N,N′*-dimethyl- and *N,N′*-dibutylquinacridone solutions, the 0-0, 0-1 and 0-2 bands appear at nearly identical wavelengths, with the 0-0 transition located at wavelengths of 524 nm (DMQA) and 525 nm (DBQA). Our measured spectra of DMQA and DBQA in DMSO match well the reported spectra for solutions of the materials in DMSO and chloroform[34,58,59] while slightly shifted spectra have been reported for solutions in various other solvents.[51,54,58,60] In comparison to the other two derivatives, *N,N′*-diphenylquinacridone in DMSO shows a blueshift of the absorption bands by *ca.* 10 nm with its absorption maximum at 514 nm. This is in good agreement with the spectrum reported by Jia *et al.* for DPQA in dichloromethane with an absorption maximum at 509 nm.[61] These trends of the optical energy gaps upon substitution are in good agreement with the trend of the electrochemical HOMO–LUMO differences determined *via* CV as shown in Fig. 2. The PL spectra of the three *N,N′*-substituted quinacridones in DMSO solution mirror the absorption spectra with a similar vibronic intensity pattern. All three compounds show Stokes shifts of *ca.* 15 nm in dilute solution.

The absorption spectra of the *N,N′*-substituted quinacridone thin films show a similar absorption band pattern as in solution in DMSO with a well-defined vibronic structure of the bands. In comparison to the DMSO solutions, the absorption spectra of all three compounds are slightly redshifted in vacuum processable thin film samples with the absorption maxima at wavelengths of 538 nm (DMQA), 526 nm (DBQA) and 522 nm (DPQA), respectively. DMQA thin film thus displays the largest redshift of the absorption bands of 14 nm in comparison to its solution. The measured absorbance spectra of *N,N′*-dimethyl- and *N,N′*-dibutyl quinacridone thin films are in good agreement with previous reports for DMQA[52,62] and DBQA.[59]

Table 1 Spectral positions and assignment of selected IR absorption bands of the *N,N′*-substituted quinacridone derivatives as shown in Fig. 3. Band assignments are based on characteristic group frequencies and assignments reported for similar molecules.[54–57] ν and δ refer to stretching and bending vibration modes, respectively. The index "oop" denotes out-of-plane vibrations

Band wavenumber/cm^{-1}			
DMQA	DBQA	DPQA	Assignment
3108, 3079, 3060	3108, 3072, 3044	3100, 3073, 3044	ν(C–H_{arom})
2933, 2918, 2833	2958, 2927, 2862		ν(C–H_{alkyl}), alkyl substituent
1620	1620	1627	ν(C═O)
1598	1602	1605	ν(C═C_{arom})
		1569	ν(C═C_{arom}), phenyl substituent
1500, 1450	1487, 1450	1482, 1448	ν(C═C_{arom}), δ(C–H)
	1443		δ(C–H_{alkyl}), butyl substituent
1428			δ(C–H_{alkyl}), methyl substituent
743, 719, 704, 608	750, 723, 710, 615	751, 713, 694, 604	δ_{oop}(C–H_{arom}), ring bending
		536	Ring deformation, phenyl substituent

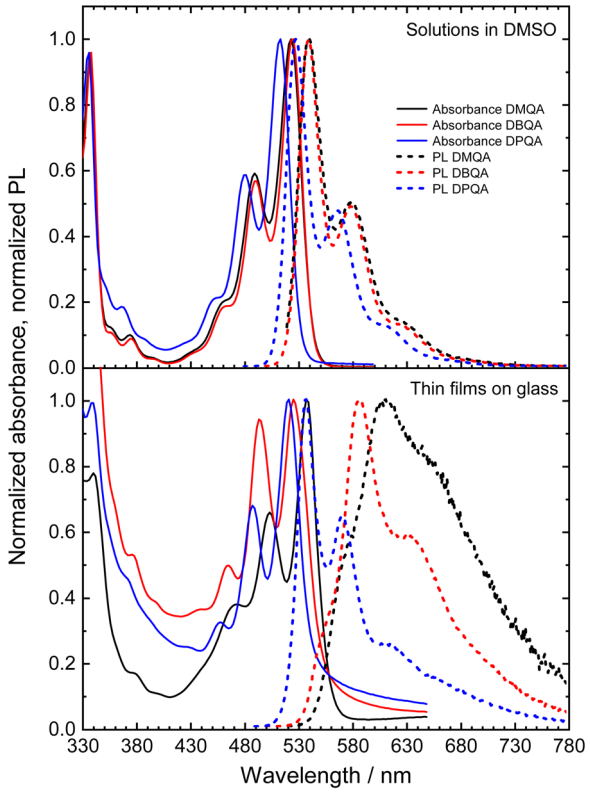

Fig. 4 Normalized absorbance and photoluminescence spectra of the *N*,*N*′-substituted quinacridones in dilute solutions (10^{-5} M) in DMSO (upper panel) and thin films deposited on quartz glass by thermal evaporation (lower panel). The PL spectra were measured at an excitation wavelength of 470 nm. The film thicknesses were 130 nm for DMQA, 140 nm for DBQA and 55 nm for DPQA.

The PL properties of the *N*,*N*′-substituted quinacridone in vacuum processable thin films clearly differ in comparison to the solutions in DMSO as evident from the significantly different spectral shapes and peak patterns among the three materials. The *N*,*N*′-dimethylquinacridone thin film shows a strongly red-shifted PL spectrum with a large Stokes shift of *ca.* 75 nm and a strong, broad tail towards the NIR wavelength regime. The maximum peak of the PL for DMQA is at a wavelength of 610 nm. Additionally, a weak shoulder peak at 575 nm and a more pronounced shoulder peak at 650 nm are visible. This pattern corresponds to the vibronic peak progression of the chromophore. The thin film of DBQA shows a more clearly defined pattern of peaks, with its PL maximum at 588 nm, a second peak at 630 nm and a weak shoulder at 550 nm. Similar to the DMQA film, the dibutyl-substituted derivative also shows a broad emission feature tailing towards the NIR wavelength region, albeit with a significantly lower relative intensity as compared to DMQA. For the DPQA thin film, the PL spectrum resembles very closely the emission spectrum of the material in DMSO solution with a well-resolved vibronic peak progression, mirroring the absorption bands, and a small Stokes shift of 16 nm. Furthermore, a very weak tailing towards the NIR regime can be observed, which is absent for the solution in DMSO. The positions of the PL peaks for the DPQA thin film are 538 nm, 572 nm, and 616 nm. For all films, the influence of self-absorption of the emitted fluorescence should be considered due to the overlap of the high energy part of the PL spectra with the absorption spectra of the materials. This may account for a decreased relative intensity of the lowest-wavelength peaks (575 nm for DMQA, 550 nm for DBQA and 538 nm for DPQA), particularly for DMQA and DBQA due to the higher film thicknesses of the investigated samples of 130 nm and 140 nm, respectively, as compared to *ca.* 55 nm for DPQA. A comparison of the PL spectral shapes of the thin films with the emission of isolated molecules in dilute DMSO solution, when accounting for the spectral redshift of the thin film PL spectra, is shown in Fig. S1 (ESI†). The comparison reveals an increasing contribution of a broad low-energy emission feature in the sequence of DPQA, DBQA to DMQA in their thin film PL spectra. The high-wavelength broad PL feature may be attributed to the emission of strongly π–π interacting species in the films.[49,59,63,64] This is corroborated by the observations of Fan *et al.*[49] and Ye *et al.*,[59] who reported PL spectra with similar shapes for polymorphs of DBQA with strong intermolecular π–π interactions. Our experimental observations thus suggest a relatively strong degree of intermolecular π–π interactions for thin film samples of DMQA, whereas DBQA shows a significantly lower degree of π–π interactions. Only a minor contribution of additional low-energy emission is found for DPQA. Furthermore, the *N*,*N*′-dimethylquinacridone film shows a heavily decreased PL intensity (peak intensity decreased by a factor of *ca.* 8.9) measured for the DMQA film in comparison with the DBQA film, which shows comparable absorbance and absorption–emission overlap, as shown in Fig. S2 (ESI†). This is a further indication of stronger π–π interactions in DMQA which may significantly decrease the PL efficiency, *e.g.* by excimer formation.[59] It should be noted that a similar high-wavelength broad PL feature was not observed for more concentrated solutions of DMQA and DBQA as shown in Fig. S3 and S4 (ESI†). However, the rather low solubilities of the materials likely limit the possibility for the observation of significant π–π interactions in the solution phase as the necessary concentrations may not be reached. For the more concentrated solutions, however, the occurrence of self-absorption can be observed by the decrease of the relative intensity of the highest energy PL peak. Despite the self-absorption, no deviation of the PL shapes in the low-energy tails can be observed, suggesting that the broad low-energy PL feature observed for the thin film samples does not originate mainly from self-absorption.

To gain further insight into the contributions of different emitting species to the PL spectra of the three *N*,*N*′-substituted quinacridones, time-resolved PL measurements were performed *via* time-correlated single photon counting (TCSPC). The PL decay curves measured at various emission wavelengths for the three compounds in solutions in DMSO and evaporated thin films on quartz glass, respectively, are displayed in Fig. 5. The decay curves were fitted by exponential functions as described in the ESI.† The parameters obtained for the fitting functions are summarized in Table S1 (ESI†). The DMSO solutions of the three compounds (Fig. 5a–c) show a mono-

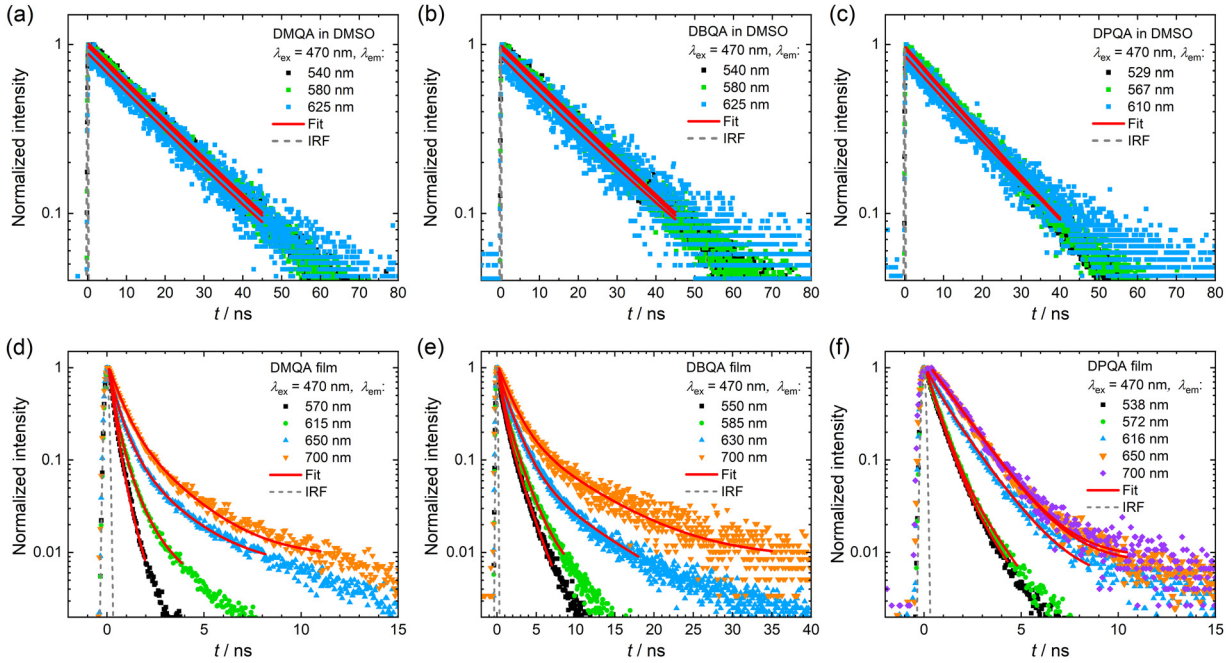

Fig. 5 Normalized PL decay curves measured for the three *N*,*N*′-substituted quinacridone derivatives in dilute DMSO solution (a–c) and thin films on quartz glass (d–f). For each sample, the wavelength at which the emission was detected was varied, while an excitation wavelength of 470 nm was used for all measurements. The decay curves were fitted with exponential functions (solid red lines) as described in the ESI.† The dashed grey curves represent the instrument response function (IRF) of the used TCSPC setup.

exponential PL decay behavior with decay time constants of 18.67 ns for DMQA, 18.92 ns for DBQA and 16.53 nm for DPQA. For the solutions of the three derivatives, no dependence of the decay time on the emission wavelength was observed.

The thin films of the three substituted quinacridones (see Fig. 5d–f) show significantly decreased decay times and the shapes of the decay curves differ from the mono-exponential type of decay observed for the solutions in DMSO. The decay curves of the DMQA and DBQA thin films were fitted by bi- or tri-exponential functions, respectively. For each material, the decay curves could be fitted with the same set of decay time constants, suggesting the occurrence of a combination of the same decay processes with different amplitudes across the measured emission wavelengths. For both DMQA and DBQA, the decay curves measured at the lowest wavelength (DMQA: 570 nm, DBQA: 550 nm) and highest wavelength (700 nm), respectively, showed a bi-exponential decay behavior. The vanishing of the slow decay component τ_3 at the lowest wavelength emission and the absence of the fast decay component τ_1 for the high wavelength emission could be observed for both materials. For the decay at the intermediate wavelengths, a more complex decay behavior consisting of three decay components was found. With increasing emission wavelength, the contribution of the longer decay components significantly increases. For DMQA, the decay time constants determined from the fits were τ_1 = 0.24 ns, τ_2 = 0.59 ns, and τ_3 = 2.07 ns. The fits for the DBQA film showed larger decay time constants of τ_1 = 0.55 ns, τ_2 = 1.67 ns, and τ_3 = 7.17 ns. The film of DPQA showed an almost identical bi-exponential decay behavior at the first two emission peaks at 538 nm and 572 nm, respectively, with time constants of τ_1 = 0.58 ns and τ_2 = 1.49 ns. For the low-energy emission of DPQA at wavelengths of 650 nm and 700 nm, the fast decay component vanishes, resulting in a mono-exponential decay behavior.

The longer-lived decay components observed for the *N*,*N*′-substituted quinacridone films may be attributed to a contribution of emission from π–π interacting molecular species (*e.g.* excimers or self-trapped excitons), which typically show prolonged lifetimes.[63–65] The faster PL decay contributions may be attributed to monomeric PL emission and fast energy transfer processes such as the population of energetically lower-lying states, such as those formed by π–π interaction of the molecules.[63,64] Furthermore, an influence of the self-absorption of the emitted PL on the PL decay behavior should be considered, which may contribute to the fast decay process observed for low emission wavelengths while prolonging the decay time at higher-wavelength emission.[66]

The emission wavelength-dependence of PL decay and long-lived component at high emission wavelengths measured for the sample thin films further suggest redshifted emission due to π–π interactions in the films as the origin of the additional broad emission feature observed in steady-state PL measurements (Fig. S1, ESI†). Due to the different relative intensities of the low-energy emission feature, the three quinacridone derivatives may be classified according to the degree of π–π interactions of the molecules in the thin films. Our experimental data thus indicate the highest degree of π–π interactions for dimethyl-substituted quinacridone which shows the largest contribution of broad, low-energy emission. For the DPQA films, the steady-state and time-resolved PL spectra indicate the dominance of a molecular packing which shows hardly any

π–π interactions and thus shows a monomeric emission similar to its dilute solution in DMSO. Since the degree of π–π interactions in an organic semiconductor is of essential importance for its charge transport properties,[67] differences in the π–π interactions among the films of three materials may have large implications for their performances as semiconducting materials in OFETs.

OFETs with *N*,*N*′-substituted quinacridones were fabricated on aluminum oxide dielectric capped by a thin layer, *i.e.* 20 nm tetratetracontane deposited *via* physical vapor deposition for dimethyl- and dibutylquinacridone on one hand and ∼12 nm beeswax (doctor bladed from 2 mg ml^{-1} solution in chloroform) for DPQA on the other hand. The ∼16 nm thick aluminum oxide layer was generated *via* anodization, through a method reported previously.[45,46] Since the anodization voltage was set to 10 V, it was expected that the aluminum oxide started leaking at applied gate voltages in excess of 5 V.[43] Nevertheless, the presence of the capping layer (in our case TTC for DMQA and DBQA and beeswax for DPQA) helped to provide an additional barrier to leakage. We could scan our devices up to −7 V and −8 V for dimethyl- and dibutyl-quinacridone, respectively (*i.e.* with 20 nm TTC capping layer), and up to −10 V for diphenyl-quinacridone (*i.e.* with ∼12 nm beeswax capping layer), albeit with a much visible leakage current for the latter. It is worth mentioning that among the three materials investigated in this work, the DPQA did not produce semiconductor characteristics when deposited on the TTC capping layer, regardless of our effort: slow *versus* fast evaporation to induce various grain sizes of diphenyl-quinacridone, and slow *versus* fast aluminum or gold source and drain electrodes deposition. We therefore varied the dielectric capping layer, investigating with this respect not only the hydrophobic TTC, as already mentioned, but also other layers of different surface polarity as for example hydrophilic shellac resin[68] or fir resins,[69] but all efforts proved unsuccessful. It is worth mentioning that diphenylquinacridone was the molecule the most difficult to control during the evaporation, with deposition rates arbitrarily and significantly fluctuating along the mean value of 0.1 A s^{-1}. That represented a flat and smooth rate for the other two cousin molecules investigated in this study. We finally centered our attention onto developing *N*,*N*′-diphenylquinacridone onto other hydrophobic dielectric capping layers and we selected beeswax as an alternative,[47,48] which seemed to have been successful at least and allowed us to measure two working OFET devices. On the other hand, DBQA and DMQA deposited on vacuum-processed TTC, produced with high reproducibility from batch to batch fabrication of the characteristics of the transistors that are presented in Fig. 6. Interestingly though, DMQA and DPQA behave as ambipolar semiconductors when capped by gold source and drain electrodes and measured in a wide voltage window as it is demonstrated in Fig. 6, while DBQA acts only as a unipolar p-type semiconductor. The ambipolar feature of the former two *N*,*N*′-substituted quinacridones (DMQA and DPQA) is clearly visible in the output characteristics, Fig. 6b and Fig. S5a (ESI†), through the super linear regime occurring at low applied gate voltages. DBQA on the other hand showed less impressive semiconductor behavior, with relatively large hysteresis and only 15 nA drain current at a

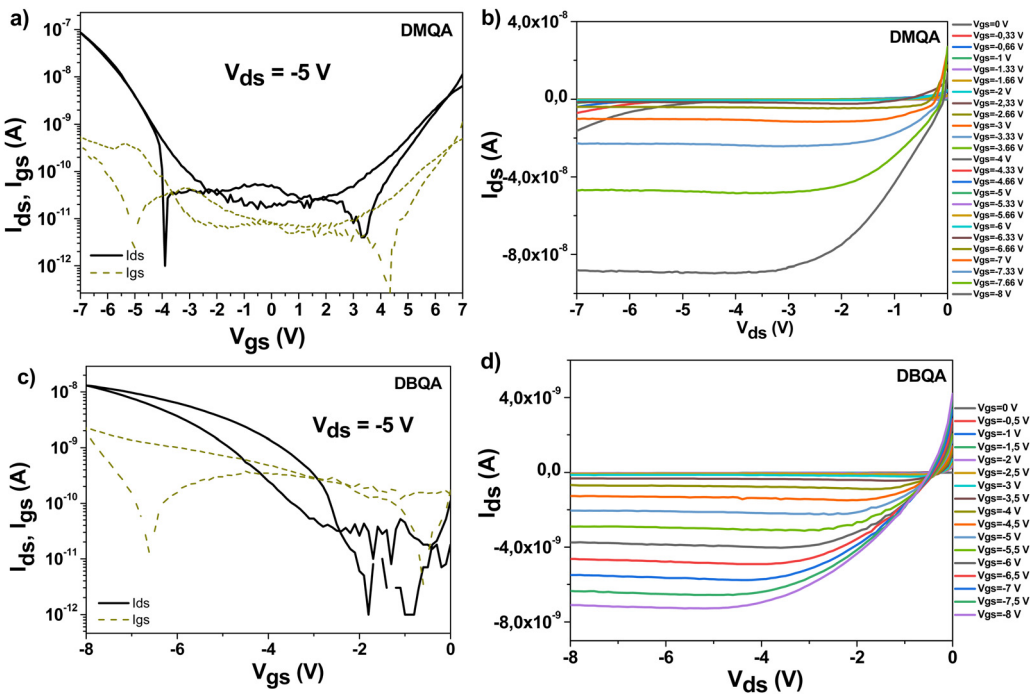

Fig. 6 OFET characteristics of *N*,*N*′ substituted quinacridones: (a) transfer and (b) output characteristics of *N*,*N*′-dimethylquinacridone. Field effect mobilities: μ_h = 8 × 10^{-3} cm^2 V^{-1} s^{-1}, μ_e = 3 × 10^{-4} cm^2 V^{-1} s^{-1}; (c) transfer and (d) output characteristics of *N*,*N*′-dibutylquinacridone. Field effect mobility μ_h = 2 × 10^{-4} cm^2 V^{-1} s^{-1}. The specific capacitance of the AlO_x + TTC is 103 nF cm^{-2}.

Table 2 Semiconductors figures of merit: electron (e^-) and hole (h^+) field effect mobilities, ON–OFF ratio (I_{ON}/I_{OFF}) and threshold voltage (V_{th})

	Field-effect mobility ($cm^2\ V^{-1}\ s^{-1}$)		I_{on}/I_{off}		V_{th} (V)	
Semiconductor	e^-	h^+	e^-	h^+	$V_{th\text{-}e}$	$V_{th\text{-}h}$
DMQA (72 working devices)	$8 \times 10^{-3} \pm 1 \times 10^{-3}$	$3 \times 10^{-4} \pm 2 \times 10^{-4}$	980	4500	4	−4.8
DBQA (72 working devices)	—	$2 \times 10^{-4} \pm 9 \times 10^{-5}$	—	1050	—	−3.5
DPQA (2 working devices)	6×10^{-6}	2×10^{-5}	16	109	−0.7	−6.2

maximum applied gate voltage of −8 V, visible in Fig. 6c. The output characteristics of *N*,*N*′-diphenylquinacridone showed good saturation and spread between successively applied gate voltages, but also because of the higher applied drain and gate voltages in excess of 5 V, the device presented also a significant leakage, visible in the output characteristics as the cross-sign crossing of the output characteristics (Fig. S5a and b, ESI†).

We investigated the ambipolarity for DBQA but could not record the *n*-channel transport even when the contact S-D electrodes were aluminum (100 nm) or LiF/Al (1 nm/99 nm).

The data comprising the OFET measurements are presented in Table 2.

Mainly because of the difficulties in establishing a reliable avenue to fabricate OFETs with DPQA, we run a series of XRD experiments in order to understand better the behavior of the respective molecule in comparison to the other two *N*,*N*′-substituted quinacridones. In Fig. 7 the XRD-measurements of the three films are displayed and compared to calculated powder diffraction reflexes and (*hkl*)-values are suggested for the measured distinct spectral features.

Initially, to build a 3-dimensional structure model of the DMQA molecule, the CIF file provided by ref: J. Mizuguchi and T. Senju[70] was considered. In the case of the DBQA, the 3-dimensional structure information is deduced from the Crystallography Open Database (COD) under the identification and "entry 1506361".[71] Based on the atomic point coordinates for these two molecules, we used "VESTA" free software in order to create a 3-dimensional crystal unit cell and calculated the corresponding X-ray powder diffractogram. Due to the fact that DPQA ($C_{32}H_{20}N_2O_2$) does not exist in the commonly accessible databases with a full set of information, a flat single molecule was built with a custom program (Java/Eclipse) and transformed into Cartesian space point coordinates for each atom of a primitive (P1) crystal unit cell in absence of any rotation

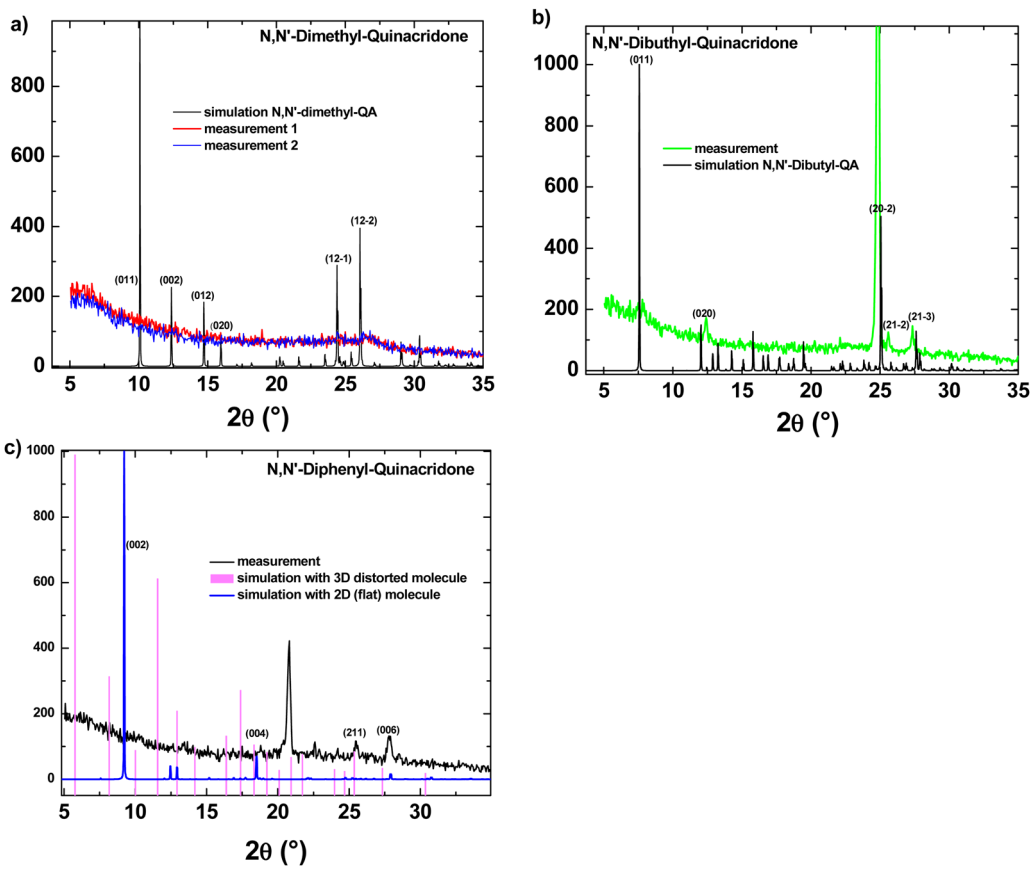

Fig. 7 Measured and simulated XRD spectra of (a) DMQA, (b) DBQA, (c) DPQA.

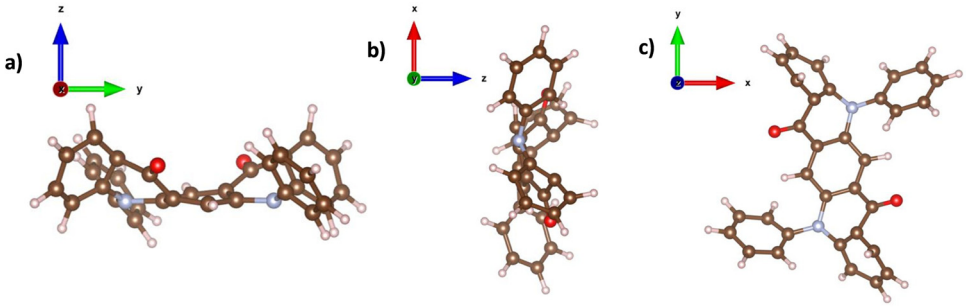

Fig. 8 The DPQA molecule in the (a) *YZ*, (b) *XZ* and (c) *XY* planes, all showing a clear distortion of its planarity.

axis. Surprisingly, accounting for the interatomic interaction forces in 3D, the whole DPQA-single molecule has been shown to be distorted, which is against the expectations, that only the phenyl groups are rotated at a 90° angle with respect to the QA-torso. In Fig. 8, the result can be found in a stick-and-ball model displayed along *a*-, *b*-, and *c*-axis. On that basis, powder diffraction Bragg reflexes under a given X-ray K_α were calculated. The two results for DPQA, one for assuming a flat molecular cell and the other accounting for the distortion, are plotted together with the experimental 2θ spectrum in Fig. 7c. A possible explanation for the poor performance of the DPQA may indeed be its non-planarity, as the XRD simulations displayed in Fig. 8 clearly show.

Conclusions

The electrochemical characterization of the three *N*,*N*′-substituted quinacridones shows that their reduction potentials (LUMO) are quite similar. In addition, no re-reduction was observed for DPQA, apparently indicating that for DPQA an irreversible oxidation reaction occurs. On the other hand, the DBQA shows high reduction current where no reductive peak is established. The DBQA also shows one oxidation peak resolved, whereas the other two pigments (DMQA and DPQA) show two peaks. The field effect mobilities measured for the OFET fabricated from these quinacridone derivatives reported in this study are not as high as pristine quinacridone,[20,72,73] probably due to the disruption of the intermolecular hydrogen bonding by substituting at the secondary amine *N*,*N*′ positions. The results show however that they still function as semiconductors in organic field effect transistor devices, and barely working devices can even be fabricated for DPQA for which a severe distortion from the planarity is induced by the two phenyl rings anchored in the *N*,*N*′ positions. The determined field effect mobilities are significantly different among the three materials, with DMQA showing the highest mobility, followed by DBQA and finally DPQA with far lower mobility. The spectroscopic characterization of the thin films of the three derivatives shows that the three materials differ strongly in their photoluminescence behavior albeit showing very similar absorption spectra. As shown by steady-state and time-resolved PL measurements, the three materials show a clearly different degree of broad, redshifted emission from π–π interacting species in their films. While for DMQA the emission from π–π interacting molecular aggregates is a dominant PL contribution, its contribution is smaller for DBQA and only very weakly observable for DPQA, where the PL is rather dominated by monomer emission. This trend can be related to a decreasing degree of π–π interactions in the thermally evaporated films when going from dimethyl to dibutyl and diphenyl substitution at the *N*,*N*′ positions in quinacridone. The trend of lower degree of π–π interactions perfectly matches the trend of the charge carrier mobilities determined from the fabricated OFET devices.

Conflicts of interest

There are no conflicts to declare.

Acknowledgements

Felix Mayr gratefully acknowledges financial support from the Austrian Research Promotion Agency (FFG) within the program e!MISSION Austria (Project Plas-Ion-PhotoKat, Grant No. 888408). Kamil Kotwica acknowledges the support of the National Science Centre of Poland, grant no. 2019/32/C/ST5/00179; Cristian Vlad Irimia acknowledges the support from the Austrian Research Promotion Agency (FFG), within the program "Talente praktika für SchülerInnen", project AQDerivaten22.

References

1 *Green Materials for Electronics*, ed. M. Irimia-Vladu, E. D. Glowacki, N. S. Sariciftci and S. Bauer, Wiley-VCH, 2017.
2 *Semiconducting and Metallic Polymers*, ed. A. J. Heeger, N. S. Sariciftci and E. B. Namdas, Oxford University Press, 2010.
3 W. A. Atherton, Miniaturization of Electronics, in *From Compass to Computer*, Palgrave, London, 1984, DOI: 10.1007/978-1-349-17365-5_10.
4 R. He, H. Liu and Y. Niu, *et al.*, Flexible Miniaturized Sensor Technologies for Long-Term Physiological Monitoring, *npj Flexible Electron.*, 2022, **6**, 20, DOI: 10.1038/s41528-022-00146-y.
5 J. Kim, R. Ghaffari and D. H. Kim, The quest for miniaturized soft bioelectronic devices, *Nat. Biomed. Eng.*, 2017, **1**, 0049, DOI: 10.1038/s41551-017-0049.

6 H. Song and G. Luo, *et al.*, Highly-integrated, Miniaturized, Stretchable Electronic Systems Based on Stacked Multilayer Network Materials, *Sci. Adv.*, 2022, **8**, eabm3785.
7 M. Kaltenbrunner, T. Sekitani, J. Reeder, T. Yokota, K. Kuribara, T. Tokuhara, M. Drack, R. Schwödiauer, I. Graz, S. Bauer-Gogonea, S. Bauer and T. Someya, An Ultra-lightweight Design for Imperceptible Pastic Electronics, *Nature*, 2013, **499**(7459), 458–463.
8 P. Meredith, C. Bettinger, M. Irimia-Vladu, A. Mostert and P. Schwenn, Electronic and Optoelectronic Materials and Devices Inspired by Nature, *Rep. Prog. Phys.*, 2013, **76**, 034501.
9 B. Stadlober, M. Zirkl and M. Irimia-Vladu, The Route towards Sustainable Smart Sensors: Ferroelectric PVDF-based Materials and Their Integration into Flexible Electronics, *Chem. Soc. Rev.*, 2019, **48**, 1787–1825.
10 G. Mao, M. Drack, M. Karami-Mosammam, D. Wirthl, T. Stockinger, R. Schwödiauer and M. Kaltenbrunner, Soft Electromagnetic Actuators, *Sci. Adv.*, 2020, **6**(26), eabc0251.
11 D. K. Khatu, N. P. Maria Joseph, R. G. Khandelwal, A. N. Rao and S.-J. Kim, Tailoring Mechanical Energy Harvesting Performance of Piezoelectric Nanogenerator *Via* Intrinsic Electrical Conductivity of Ferroelectrics, *Mater. Today*, 2021, **20**, 100679.
12 S. Appusamy, S. Krishnan, M. Gopikrishna and S. Raman, Bio-based Materials for Microwave Devices: A Review, *J. Electron. Mater.*, 2021, **50**, 1893–1921.
13 P. Parzer, F. Perteneder, K. Probst, C. Rendl, J. Leong, S. Schuetz, A. Vogl, R. Schwoediauer, M. Kaltenbrunner and S. Bauer, RESi: A Highly Flexible, Pressure-sensitive, Imperceptible Textile Interface Based on Resistive Yarns, *Proceedings of the 31st Annual ACM Symposium on User Interface Software and Technology*, 2018, pp. 745–756.
14 M. Irimia-Vladu, Green Electronics: Biodegradable and Biocompatible Materials and Devices for Sustainable Future, *Chem. Soc. Rev.*, 2014, **43**, 588–610.
15 D. Martin, Polymers Manipulate Cells, *Nat. Mater.*, 2007, **6**, 626–627.
16 D. Bennet and S. Kim, Implantable Microdevice for Peripheral Nerve Regeneration: Materials and Fabrications, *J. Mater. Sci.*, 2011, **46**, 4723–4740.
17 V. Lundin, A. Herland, M. Berggren, E. W. H. Jager and A. I. Teixeira, Control of Neural Stem Cell Survival by Electroactive Polymer Substrates, *PLoS One*, 2011, **6**, e18624.
18 D. Khodagholy, T. Doublet, M. Gurfinkel, P. Quilichini, E. Ismailova, P. Leleux, T. Herve, S. Sanaur, C. Bernard and G. G. Malliaras, Highly Conformable Conducting Polymer Electrodes for In Vivo Recordings, *Adv. Mater.*, 2011, **23**, H268–H272.
19 D. H. Kim, N. S. Lu and R. Ma, *et al.*, Epidermal Electronics, *Science*, 2011, **333**, 838–843.
20 E. D. Glowacki, M. Irimia-Vladu, M. Kaltenbrunner, J. Gąsiorowski, M. S. White, G. Romanazzi, G. P. Suranna, P. Mastrorilli, T. Sekitani, S. Bauer, T. Someya, L. Torsi and N. S. Sariciftci, Hydrogen- bonded Semiconducting Pigments for Air-stable Field-effect Transistors, *Adv. Mater.*, 2013, **25**, 1563–1569.
21 G. Tian, W. Wang, B. Huang, L. Shi, L. Li, J. Xia, Y. Pan, S. Chen, T. Jia and T. Sun, A Quinacridone Derivative with Intensive Emission in Both Solution and Solid State *via* a Facile Preparation for Cell Imaging Application, *J. Mater. Chem. B*, 2019, **7**, 3192–3196.
22 A. Cetcovic, A. Bellapianta, M. Irimia-Vladu, J. Hofinger, C. Yumusak, A. Corna, M. C. Sharber, G. Zeck, N. S. Sariciftci, M. Bolz and A. Salti, In vitro Biocompatibility of D18 and Y6 as Potential Organic Semiconductors for Retinal Prosthesis, *Int. J. Mol. Sci.*, 2022, **23**, 8666, DOI: **10.3390/ijms23158666**.
23 S. S. Labana and L. L. Labana, Quinacridones, *Chem. Rev.*, 1967, **67**(1), 1–18.
24 M. Irimia-Vladu, E. D. Glowacki, N. S. Sariciftci and S. Bauer, Natural Materials for Organic Electronics, in *Small Organic Molecules on Surfaces*, ed. H. Sitter, C. Draxl and M. Ramsey, Springer Volume in Materials Science, Springer Verlag, 2013, vol. 173, pp. 295–318.
25 E. D. Glowacki and M. Irimia-Vladu, *Natural and Nature-inspired Materials in Organic Electronics*, SPIE Newsroom, 2012, DOI: **10.1117/2.1201201.004054**.
26 E. D. Glowacki, L. Leonat, M. Irimia-Vladu, R. Schwödiauer, M. Ullah, H. Sitter, S. Bauer and N. S. Sariciftci, Intermolecular Hydrogen-bonded Organic Semiconductors: Quinacridone versus Pentacene, *Appl. Phys. Lett.*, 2012, **101**, 023305.
27 S. Dunst, E. Karner, M. E. Coppola, G. Trimmel and M. Irimia-Vladu, Comparison of the Solution and Vacuum Processed Quinacridones in Homojunction Photovoltaics, *Monatsh. Chem.*, 2017, **148**(5), 863–870.
28 E. F. Paulus, F. J. J. Leusenb and M. U. Schmidt, Crystal Structures of Quinacridones, *CrystEngComm*, 2007, **9**, 131–143.
29 G. Linke, A Review of Thirty Years of Research on Quinacridones. X-ray Crystallography and Crystal Engineering, *Dyes Pigm.*, 2000, **44**, 101–122.
30 G. Linke, On Quinacridones and Their Supramolecular Mesomerism Within the Crystal Latice, *Dyes Pigm.*, 2002, **52**, 169–181.
31 E. D. Głowacki, M. Irimia-Vladu, S. Bauer and N. S. Sariciftci, Hydrogen-bonds in Molecular Solids - from Biological Systems to Organic Electronics, *J. Mater. Chem. B*, 2013, **1**, 3742–3753.
32 M. Jakešová, D. H. Apaydin, M. Sytnyk, K. Oppelt, W. Heiss, N. S. Sariciftci and E. D. Głowacki, Hydrogen-Bonded Organic Semiconductors as Stable Photoelectrocatalysts for Efficient Hydrogen Peroxide Photosynthesis, *Adv. Funct. Mater.*, 2016, **26**, 5248–5254.
33 S. Ito, G. Katada, T. Taguchi, I. Kawamura, T. Ubukata and M. Asami, Tricolor Mechanochromic Luminescence of an Organic Two-component Dye: Visualization of a Crystalline State and Two Amorphous States, *CrystEngComm*, 2019, **21**, 53–59.
34 T. Tsutsui, S. Kusaba, M. Yamashina, M. Akita and M. Yoshizawa, Open versus Closed Polyaromatic Nanocavity: Enhanced Host Abilities toward Large Dyes and Pigments, *Chem. – Eur. J.*, 2019, **25**, 4320–4324.

35 M. Shen, X. Zhao, L. Han, N. Jin, S. Liu, T. Jia, Z. Chen and X. Zhao, Developing Flexible Quinacridone-Derivatives-Based Photothermal Evaporaters for Solar Steam and Thermoelectric Power Generation, *Chem. – Eur. J.*, 2022, **28**, e202104137.
36 C. Sakong, S. H. Kim, S. B. Yuk, J. Y. Kim, S. W. Park, M. J. Ko and J. P. Kim, Synthesis of Novel Quinacridone Dyes and Their Photovoltaic Performances in Organic Dye-sensitized Solar Cells, *Bull. Korean Chem. Soc.*, 2011, **32**(8), 2553–2559.
37 Z.-X. Xu, H.-F. Xiang, V. A. L. Roy, S. S.-Y. Chui, Y. Wang, P. T. Lai and C.-M. Che, Organic Field-effect Transistors Fabricated with N,N-substituted Dialkyl-1,3,8,10-tetramethylquinacridone Compounds, *Appl. Phys. Lett.*, 2009, **95**, 123305.
38 R. C. Pereira, A. D. R. Pontinha, M. Pineiro and J. S. Seixas de Melo, A Comprehensive Spectral, Photophysical and Electrochemical Study of Synthetic Water-soluble Acridones. A New Class of pH and Polarity Sensitive Fluorescent Probes, *Dyes Pigm.*, 2010, **166**, 203–210.
39 H. C. Song, Y.-W. Chen, X. L. Zheng and B. N. Ying, Study on Second Harmonic Generation of 10-Hydrocarbylacridones, *Spectrochim. Acta, Part A*, 2001, **57**(9), 1717–1723.
40 A. Boużyk, L. Jóźwiak, A. Yu Kolendo and J. Błażejowski, Theoretical interpretation of electronic absorption and emission transitions in 9-acridinones, *Spectrochim. Acta, Part A*, 2003, **59**(3), 543–558.
41 J. E. Anthony, C. R. Swartz, C. A. Landis and S. R. Parkin, Synthesis, Optical, Thermal, and Redox Properties of 2,3,9,10-tetrasubstituted-6,13-dialkynylpentacenes, *Proc. SPIE*, 2005, **5940**, 594002.
42 Q. Miao, X. Chi, S. Xiao, R. Zeis, M. Lefenfeld, T. Siegrist, M. L. Steigerwald and C. Nuckolls, Organization of Acenes with a Cruciform Assembly Motif, *J. Am. Chem. Soc.*, 2006, **128**(4), 1340–1345.
43 C. Yumusak, N. S. Sariciftci and M. Irimia-Vladu, Purity of Organic Semiconductors as a Key Factor for the Performance of Organic Electronic Devices, *Mater. Chem. Front.*, 2020, **4**, 3678–3689.
44 N. G. Connelly and W. E. Geiger, Chemical Redox Agents for Organometallic Chemistry, *Chem. Rev.*, 1996, **96**, 877–910.
45 L. A. Majewski, M. Grell, S. D. Ogier and J. Veres, A Novel Gate Insulator for Flexible Electronics, *Org. Electron.*, 2003, **4**, 27–32.
46 M. Irimia-Vladu, P. A. Troshin, M. Reisinger, G. Schwabegger, M. Ullah, R. Schwoediauer, A. Mumyatov, M. Bodea, J. W. Fergus, V. F. Razumov, H. Sitter, S. Bauer and N. S. Sariciftci, Environmentally Sustainable Organic Field-effect Transistors, *Org. Electron.*, 2010, **11**, 1974–1990.
47 B. Stadlober, E. Karner, A. Petritz, A. Fian and M. Irimia-Vladu, Nature as Microelectronic Fab: Bioelectronics: Materials, Transistors and Circuits, *IEEE J. Solid-State Circuits*, 2015, **41**, 10–17.
48 M. Baumgartner, M. E. Coppola, N. S. Sariciftci, E. D. Głowacki, S. Bauer and M. Irimia-Vladu, Emerging "Green" Materials and Technologies for Electronics, in *Green Materials for Electronics*, ed. M. Irimia-Vladu, E. D. Glowacki, N. S. Sariciftci and S. Bauer, Wiley-VCH, 2017.
49 Y. Fan, Y. Zhao, L. Ye, B. Li, G. Yang and Y. Wang, Polymorphs and Pseudopolymorphs of *N*,*N*-Di(*n*-butyl) Quinacridone: Structures and Solid-State Luminescence Properties, *Cryst. Growth Des.*, 2009, **9**(3), 1421–1430.
50 I. Javed, A. Khurshid, M. N. Arshad and Y. Wang, Photophysical And Electrochemical Properties and Temperature Dependent Geometrical Isomerism In Alkyl Quinacridonediimines, *New J. Chem.*, 2014, **38**, 752–761.
51 J. Zhang, F. Dumur, M. Bouzrati, P. Xiao, C. Dietlin, F. Morlet-Savary, B. Graff, D. Gigmes, J. P. Fouassier and J. Lalevee, Novel Panchromatic Photopolymerizable Matrices: *N*,*N*′-Dibutylquinacridone as an Efficient and Versatile Photoinitiator, *J. Polym. Sci., Part A: Polym. Chem.*, 2015, **53**(14), 1719–1727.
52 M. Socol, N. Preda, C. Breazu, C. Florica, A. Costas, C. M. Istrate, A. Stanculescu, M. Girtan and F. Gherendi, Organic Heterostructures Obtained on ZnO/Ag/ZnO Electrode, *Vacuum*, 2018, **154**, 366–370.
53 D.-S. Leem, K.-H. Lee, K.-B. Park, S.-J. Lim, K.-S. Kim, Y. W. Jin and S. Lee, Low Dark Current Small Molecule Organic Photodetectors with Selective Response to Green Light, *Appl. Phys. Lett.*, 2013, **103**, 043305.
54 E. del Puerto, C. Domingo, S. Sanchez-Cortez, J. V. García-Ramos and R. F. Aroca, Plasmon Enhanced Spectroscopy of *N*,*N*′-Dialkylquinacridones Used as Codopants in OLEDs, *J. Phys. Chem. C*, 2011, **115**, 16838–16843.
55 M. A. Palafox, Scaling Factors for the Prediction of Vibrational Spectra. I. Benzene Molecule, *Int. J. Quantum Chem.*, 2000, **77**, 661–684.
56 S. Enengl, C. Enengl, P. Stadler, H. Neugebauer and N. S. Sariciftci, Spectroelectrochemical Studies on Quinacridone by Using Poly(vinyl alcohol) Coating as Protection Layer, *Chem. Phys. Chem.*, 2015, **16**, 2206–2210.
57 P. M. Wojciechowski, W. Zierkiewicz, D. Michalska and P. Hobza, Electronic structures, vibrational spectra, and revised assignment of aniline and its radical cation: Theoretical study, *J. Chem. Phys.*, 2003, **118**, 10900–10911.
58 J. Mizuguchi and T. Senju, Solution and Solid-State Spectra of Quinacridone Derivatives as Viewed from the Intermolecular Hydrogen Bond, *J. Phys. Chem. B*, 2006, **110**, 19154–19161.
59 K. Ye, J. Wang, H. Sun, Y. Liu, Z. Mu, F. Li, S. Jiang, J. Zhang, H. Zhang, Y. Wang and C. Che, Supramolecular Structures and Assembly and Luminescent Properties of Quinacridone Derivatives, *J. Phys. Chem. B*, 2005, **109**, 8008–8016.
60 H. Bi, K. Ye, Y. Zhao, Y. Yang, Y. Liu and Y. Wang, Fluorinated Quinacridone Derivative Based Organic Light-Emitting Device with High Power Efficiency, *Org. Electron.*, 2010, **11**, 1180–1184.
61 J. Jia, D. Feng, Y. Sha, C. Zhou, G. Liang and Y. She, New Quinacridone Derivatives: Synthesis, Photophysical and Third-Order Nonlinear Optical Properties, *Tetrahedron*, 2020, **76**, 131057.
62 K.-H. Lee, D.-S. Leem, S. Sul, K.-B. Park, S.-J. Lim, H. Han, K.-S. Kim, Y.-W. Jin, S. Lee and S. Y. Park, A High Performance Green-Sensitive Organic Photodiode Comprising A Bulk Heterojunction of Dimethyl-Quinacridone and Dicyanovinyl Terthiophene, *J. Mater. Chem. C*, 2013, **1**, 2666–2671.

63 O. P. Dimitriev, Y. P. Piryatinski and Y. L. Slominskii, Excimer Emission in J-Aggregates, *J. Phys. Chem. Lett.*, 2018, **9**, 2138–2143.
64 Y. Kim, J. Bouffard, S. E. Kooi and T. M. Swager, Highly Emissive Conjugated Polymer Excimers, *J. Am. Chem. Soc.*, 2006, **127**, 13726–13731.
65 J. Lee, H. Jung, H. Shin, J. Kim, D. Yokoyama, H. Nishimura, A. Wakamiya and J. Park, Excimer emission based on the control of molecular structure and intermolecular interactions, *J. Mater. Chem. C*, 2016, **4**, 2784–2792.
66 J.-F. Cormier, M. Fortin, J. Frechette, I. Noiseux, M. L. Vernon and W. Long, The effects of self-absorption and detection geometry on fluorescence intensity and decay lifetime, *Proc. SPIE*, 2005, **5702**, 123–134.
67 V. Coropceanu, J. Cornil, D. A. da Silva Filho, Y. Olivier, R. Silbey and J.-L. Bredas, Charge Transport in Organic Semiconductors, *Chem. Rev.*, 2007, **107**, 926–952.
68 M. Irimia-Vladu, E. D. Głowacki, G. Schwabegger, L. Leonat, H. Z. Akpinar, H. Sitter, S. Bauer and N. S. Sariciftci, Natural Resin Shellac As A Substrate And A Dielectric Layer For Organic Field-effect Transistors, *Green Chem.*, 2013, **15**(6), 1473–1476.
69 J. Ivic, A. Petritz, C. V. Irimia, B. Kahraman, Y. Kanbur, M. Bednorz, C. Yumusak, M. A. Aslam, A. Matkovic, K. Saller, C. Schwarzinger, W. Schühly, A. I. Smeds, Y. Salinas, M. Schiek, F. Mayr, C. Xu, C. Teichert, M. Osiac, N. S. Sariciftci, B. Stadlober and M. Irimia-Vladu, Pinaceae Fir Resins as Natural Dielectrics for Low Voltage Operating, Hysteresis-free Organic Field Effect Transistors, *Adv. Sustainable Syst.*, 2022, **6**, 2200234.
70 J. Mizuguchi and T. Senju, Reinvestigation of 5,12-dihydro-5,12-dimethylquino[2,3-*b*]acridine-7,4-dione, *Acta Crystallogr.*, 2003, **E59**, o232–o233.
71 K. Ye, J. Wang, H. Sun, Y. Liu, Z. Mu, F. Li, S. Jiang, J. Zhang, H. Zhang, Y. Wang and C.-M. Che, Supramolecular Structures and Assembly and Luminescent Properties of Quinacridone Derivatives, *J. Phys. Chem. B*, 2005, **109**(16), 8008–8016.
72 J. Mei, Y. Diao, A. L. Appleton, L. Fang and Z. Bao, Integrated Materials Design of Organic Semiconductors for Field-effect Transistors, *J. Am. Chem. Soc.*, 2013, **135**(18), 6724–6746.
73 P. Hu, X. He and H. Jiang, Greater than 10 $cm^2 V^{-1} s^{-1}$: A Breakthrough of Organic Semiconductors for Field-effect Transistors, *InfoMat*, 2021, **3**, 613–630.